Book Chapter

Analytical Determination of the Constitutive Behavior from Micro-Pillar Testing: Application to a Tempered Martensitic Steel

N Ilchuk[1,2], P Spätig[1,2]* and HP Seifert[2]

[1]Fusion Technology-Materials, CRPP EPFL, Association EURATOM-Confédération Suisse, Switzerland
[2]Laboratory for Nuclear Materials, Nuclear Energy and Safety Research Department, Switzerland

***Corresponding Author:** P Spätig, Laboratory for Nuclear Materials, Nuclear Energy and Safety Research Department, 5232 Villigen PSI, Switzerland

Published **June 15, 2020**

This Book Chapter is a republication of an article published by N Ilchuk, et al. at AIP Advances in April 2014. (N Ilchuk, P Spätig, HP Seifert. Analytical Determination of the Constitutive Behavior from Micro-Pillar Testing: Application to a Tempered Martensitic Steel. AIP Advances. 4, 047126 (2014); https://doi.org/10.1063/1.4873155.)

How to cite this book chapter: N Ilchuk, P Spätig, HP Seifert. Analytical Determination of the Constitutive Behavior from Micro-Pillar Testing: Application to a Tempered Martensitic Steel. In: Vishnu Gopal, editor. Prime Archives in Physical Sciences. Hyderabad, India: Vide Leaf. 2020.

Acknowledgement: The authors gratefully acknowledge the support of the Swiss Government through the Swiss Volontary Contribution to the Broader Approach under contract SBF ITER/BA-Project no 2009-02.

Abstract

Micro-compression experiments were carried out on micro-pillars, with nominal diameter of 10 μm and height 20 μm, and fabricated from a high-chromium tempered martensitic steels developed for nuclear applications. An analytical method was proposed to calculate the imposed compressive displacement on the pillar that allows determining the constitutive behavior up to about 5% of plastic strain. The experimental micro-compression curves were showed to be adequately modeled by the finite element simulations, which were used to validate the main assumption considered for the analytical model development.

Testing micro-pillars in compression has been becoming a common technique to investigate mechanical properties of a variety of materials. For instance, either the evolution of the mechanical response with specimen dimensions at the micron and/or submicron scale is the interest of such studies [1-4], or the motivation resides in the need to measure the local stress/strain behavior of individual phases constituents of multiphase system [5], or to determine the mechanical response locally in small irradiated specimen [6]. One of the main challenges in the determination of the true stress/strain curve from the micro-pillars is to account for their typical tapered geometry, which induced a non-uniform stress distribution through the height of the micro-pillar. Some authors deal with that problem by considering empirical techniques to average the stress [5] In this paper, we present a new method to analytically derive the true stress-strain curve from the testing of micro-pillars applied to tempered martensitic steels for nuclear structural applications.

The material selected is the high-chromium reduced activation tempered martensitic reference steel, Eurofer97, which exhibits a fully tempered martensitic microstructure [7]. Its chemical composition is (in wt%) 8.9Cr-1.07W-0.47Mn-0.2V-0.14Ta-

0.12C. The final heat-treatment was 0.5 h at 980 °C and tempering at 760 °C for 1.5 h. This steel has a homogeneous tempered martensitic microstructure with a typical structure originating from the as-quenched lath martensite (Figure 1). The plastic deformation of this steel was studied in the unirradiated condition and after a neutron irradiation, which was performed in the BAGIRA rig of the experimental reactor at AEKI-KFKI in Budapest, Hungary. The irradiation was performed at 150 °C up to a neutron fluence of 2.5×10^{20} n/cm^2 (E > 1.0 MeV; which corresponds to about 0.33 ± 0.05 dpa, *displacement per atom*). Two types of test were performed: tensile tests on small flat specimens and compression on micro-pillars produced with focused ion beam (FIB). The micro-pillars (Figure 1) were small cylinders with nominal dimensions: 10 μm in diameter and 20 μm in height (1:2 ratio). They were produced as follows. Before machining by focused-ion beam (FIB), the specimen surface was mirror-polished with diamond suspension as fine as 0.25 μm. Zeiss NVision 40 dual-beam (FIB-SEM) system equipped with a FIB column with gallium liquid metal ion source and a field-emission Scanning Electron Microscope (SEM) column was used for the micro-pillar machining. First, a pre-mill of a 20 μm wide ring with an external diameter of 100 μm using 27 nA FIB milling current and "50 μm depth" in the "feature-mill" regime results in a ~18 μm deep crater. The pre-milling step with the high beam current is required in order to reduce the overall time of the micro-pillar fabrication process. The second step is the "annular" milling of a second 35 μm wide ring with a diameter of 80 μm. The annular milling setting are: milling current is 1.5 nA with the 2048 resolution, the dwell time is the 155 ms for the outer ring to the 150 ms for the inner ring. The final shaping fine cut using the 700 pA milling current was done to minimize the tapering effect of the annular milling. This machining process was developed specifically for Eurofer97 tempered martensitic steel. The micro-compressions were carried out with a MTS Nanoindenter G200 instrument equipped with a flat diamond tip. The load-displacement data from the micro-compression tests were recorded and further used for the analysis presented hereafter.

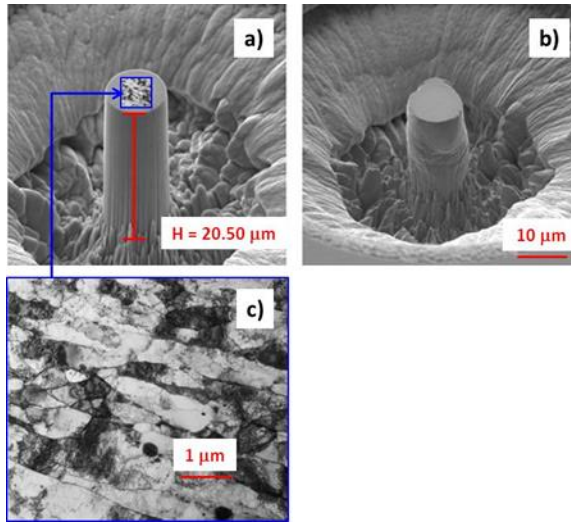

Figure 1: SEM images of typical micro-pillars FIB-machined from Eurofer97 before a) and after b) compression, and TEM micrographs c) of the tempered lath microstructure.

Finite element (FE) calculations were performed using the commercial code ABAQUS/Standard 6.12. The flat diamond tip was modeled as an axisymmetric deformable part with isotropic elastic properties, Young's modulus ($E = 1141$ GPa) and Poisson's ratio ($\nu = 0.07$). Due to the symmetry of the micro-pillar geometry only the half of the specimen was modeled with the following dimensions: 40×45 µm^2 (width × height) for the substrate part, with the pillar having the typical height of ~20 µm and a radius of ~5 µm (the exact micro-pillar specimen geometry (radius and height) was taken into account for each simulation). The specimen was meshed with 8604 four-node bilinear axisymmetric quadrilateral elements with reduced integration. In the unirradiated case, the constitutive behavior of the unirradiated Eurofer97 steel was deduced from the corresponding tensile test and used as an input to the FE micro-pillar model. However, we have shown in [8] that the tensile test after irradiation at 150 °C presents a very small uniform elongation. The constitutive behavior of irradiated Eurofer97 used as the input for the FE models was then obtained with an inverse method as described in [8]. In both cases, the plastic behavior was given in the form of tabulated true stress – true

plastic strain. The Young's modulus and Poisson's ratio of the steel were respectively 210 GPa and 0.3. The contact between the diamond tip and the micro-pillar was assumed frictionless.

Figure 2 shows a very good match between the experimental load-displacement curves of two micro-pillars in the unirradiated and irradiated Eurofer97 with their corresponding FE models. In Figure 2, it can be distinguished that the yielding for the irradiated Eurofer97 occurs as expected at a larger load in comparison with the unirradiated material, consistently with the tensile results in [8], and reflecting the well-known irradiation-hardening. While the micro-pillar testing consists in deforming small compression specimens, the conversion of the measured load-displacement curve into the true stress-strain curve is not straightforward due to the geometry of the micro-pillar. As a matter of fact, the final geometry of the micro-pillars is never a perfect cylinder. They are actually tapered, which has to be taken into account in the stress/strain analysis.

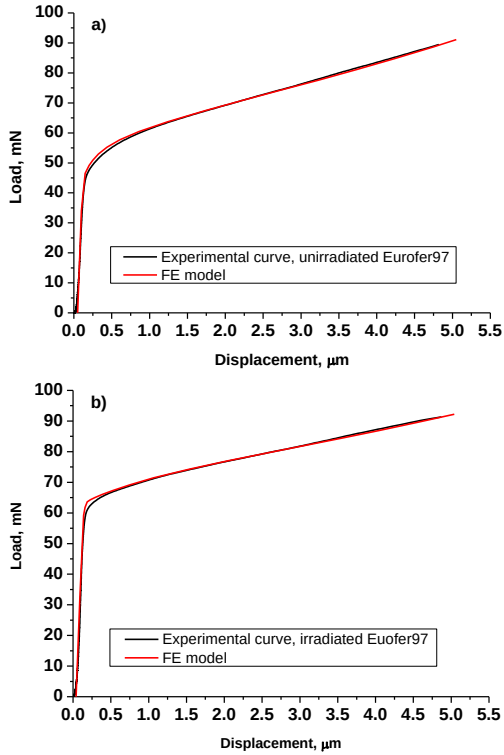

Figure 2: Typical experimental load-displacement curves of micro-pillar with the corresponding FE calculated curves. a) unirradiated Eurofer97, b) irradiated Eurofer97.

To extract the true stress-strain curve, we did the assumption that, despite the relatively small size of the specimen, the deformation behavior remains representative of the bulk. The justification is essentially based upon the fact that the basic microstructural unit of the tempered martensitic structure is the tempered lath whose dimensions are of the order of 0.5-1 μm in width and several μm in length. Thus, owing to the size of the micro-pillars used in this work, a larger number of these microstructural units are contained in the specimens (see Figure 1). In addition, the finite element simulations performed to reconstruct the load-displacement curve showed a very good agreement with experimental results. Since the finite element

simulations are based upon a continuum approach of plasticity, the good match between the simulation and experiment is an additional indication that the mechanical response of the micro-pillars remains representative of the bulk. Furthermore, it is fully consistent with the work of Shin *et al.* [9] who showed that there is no significant size effect on the measured strengths of an oxide dispersion strengthened steels down to a pillar size of 1 μm. This was attributed to the fact that the studied alloy presented possesses a fine grain structure of about 450 nm.

The model developed in this study to do the conversion from the load-displacement into the true stress-strain is presented hereafter. We followed the work of Dimiduk *et al.* [4] who developed a formula to calculate the elastic displacement of micro-pillar. However, our model is extended in the plastic range. A schematic drawing of the pillar geometry and parameters considered is shown in Figure 3. The model is based upon the fact that the main component of the stress tensor is σ_{yy}, at least in the elastic regime and for moderate plastic deformation. This point was actually verified by the finite element simulations. In Figure 4, as an example we show a micro-pillar of unirradiated Eurofer97 loaded just above the load P_y necessary to produce a general yielding on the top end of the pillar. The active plastic zone is indicated in red. The non-zero components of the stress tensor, calculated by finite element simulations for the series of element just below the indenter (Position 1 in Figure 4), are plotted against the radial distance in Figure 5. It is clear that σ_{yy} dominates all the other components and that each component is only weakly dependent on the radial position. We also emphasize that the calculated yield load P_y, at which the plastic zone has spread through the whole diameter on the top of the pillar, is consistent with the yield stress used as input for the simulations. Indeed, P_y allows to estimate the yield stress through the equation $\sigma_y = 4P_y/\pi D_0^2$, which was equal to ~ 495 MPa, to compare with the input yield stress set at 470 MPa.

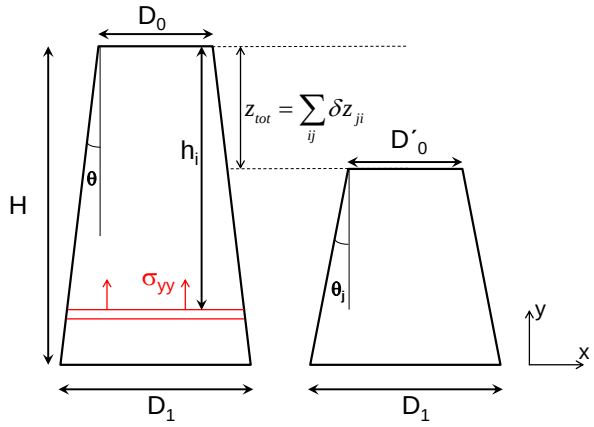

Figure 3: Parameters used to describe the micro-pillar geometry: a) undeformed micro-pillar, b) deformed micro-pillar after the jth load increment.

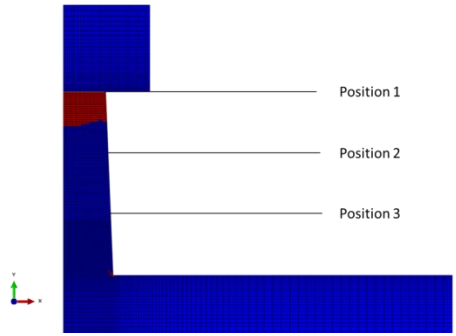

Figure 4: Active plastic zone at general yielding of unirradiated Eurofer97 micro-pillar. The positions indicate the height where the stress components, reported in Table 1, were averaged over the micro-pillar cross-section.

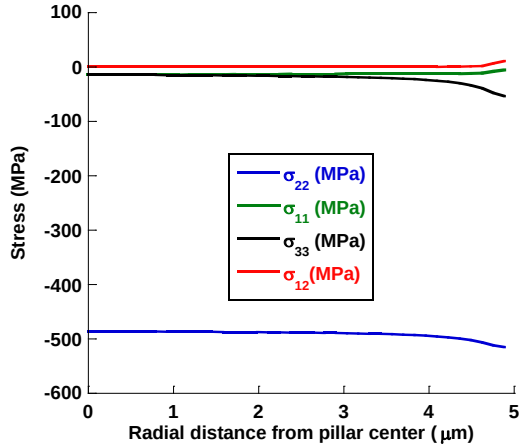

Figure 5: Radial stress distribution on the micro-pillar top end at general yielding at position 1, unirradiated Eurofer97.

In Table 1, we give the average values over the cross-section of the stress components at three different positions: 1) on the top of pillar just below the flat indenter, 2) at one third of the pillar height and 3) at two thirds of the pillar height (see Figure 4). Again, σ_{yy} calculated by FE simulations appears as the dominating component, which in addition is very well approximated by the so-called experimental normal component obtained by dividing the applied load by the actual cross-section of the layer. A similar conclusion is drawn from the irradiated micro-pillar simulations, as well as for deformation level for which the plastic zone does not extend into the substrate.

Table 1: Average stresses at three different layers of diameter D calculated by FE (see Figure 4). The experimental normal stress is also indicated for comparison with $\overline{\sigma_{22}}$.

	Experimental normal stress in MPa	FEM calculations, average stresses in three different layers in MPa			
Position	$\sigma = 4P/\pi D^2$	$\overline{\sigma_{22}}$	$\overline{\sigma_{11}}$	$\overline{\sigma_{33}}$	$\overline{\sigma_{12}}$
1	-495.0	-491.2	-12.9	-20.5	0.75
2	-442.7	-442.4	0.01	0.3	8.8
3	-396.4	-398.2	-0.9	0.2	6.9

The derivation of the true stress-strain curve is based upon a fitting procedure where the parameters of the constitutive law are adjusted to reconstruct the measured displacement of the flat tip z_{meas} as a function of the load. Actually, z_{meas} represents the sum of the displacements of the "substrate" z_s and of the pillar z_p.

$$z_{meas} = z_s + z_p \qquad (1)$$

The displacement of the substrate is estimated from Sneddon's formula as [10]:

$$z_S = \frac{P_j(1-\nu)}{2E\left(D_0+H_j tan(\theta_j)\right)} \qquad (2)$$

where j represents the j^{th} load increment, H_j the actual height of the pillar at the j^{th} load increment and ν the Poisson's ratio. The basic idea is to divide the micro-pillars in thin horizontal layers, for which the j^{th} incremental displacement can be deduced from the j^{th} incremental load. As justified above, the displacement of the pillar is obtained by assuming that the stress is uniformly distributed over the horizontal layers of the pillar. In other words, only the normal stress and strain components, σ_{yy} and ε_{yy}, are considered, which, for the sake of simplicity are simply refer as to σ and ε in the following equations. For the i^{th} layer, we note: δP_{ji}, $\delta z_{ji,p}$, $\delta\sigma_{ji}$, $\delta\varepsilon_{ji}$, the j^{th} incrementals of load, displacement, stress and strain respectively. $\delta\varepsilon_{ji}$ is is replaced by dividing the incremental stress $\delta\sigma_{ji}$ by the strain-hardening coefficient $\tilde{\Theta}_{ji}$ ($\delta\varepsilon_{ji} = \delta\sigma_{ji}/\tilde{\Theta}_{ji}$). Thus, the strain increment $\delta\varepsilon_{ji}$ depends on $\delta\sigma_{ji}$ and $\tilde{\Theta}_{ji}$ that are respectively an experimentally measurable quantity and an analytical quantity given by Eq. (8). The basic idea is then to fit the parameters of the strain-hardening law to reconstruct the measured displacement as a function of the load. The incremental stress is deduced from the incremental load δP_{ji}. So the incremental pillar displacement $\delta z_{ji,p}$ of the i^{th} layer for the j^{th} increment of load is given by:

$$\delta z_{ji,p} = t_{ji}\delta\varepsilon_{ji} = t_{ji}\frac{\delta\sigma_{ji}}{\tilde{\Theta}_{ji}} = t_{ji}\frac{4\delta P_{ji}}{\pi\tilde{\Theta}_{ji}\left(D_0+2h_{ji}tan(\theta_j)\right)^2} \qquad (3)$$

where t_{ji} is the actual thickness of the i^{th} layer at the j^{th} increment of load, and the normal stress is calculated as:

$$\sigma_{ji} = \frac{4P_{ji}}{\pi\left(D_0+2h_{ji}tan(\theta_j)\right)^2} \qquad (4)$$

The compressive *incremental displacement* of the entire micro-pillar corresponding to the j^{th} incremental applied load δP_j is obtained by adding all the incremental displacements of *i* layers as:

$$\delta z_{j,p} = \sum_i \delta z_{ji,p} \qquad (5)$$

Finally, the total compressive displacement of the entire micro-pillar at a given load is obtained by summation on all the *j* increments of load considered:

$$z_p = \sum_{ij} \delta z_{ji,p} = \sum_{ij} t_{ji} \frac{4\delta P_{ji}}{\pi\tilde{\Theta}_{ji}\left(D_0+2h_{ji}tan(\theta_j)\right)^2} \qquad (6)$$

where j represents the j[th] load increment. After each load increment, the geometry of the pillar is updated by assuming that: 1) the deformation is done at a constant volume, 2) D_1, the bottom diameter of the micro-pillar (see Figure 3) is constant. Thus D_0' and θ are recalculated for each load increment.

To extract the constitutive behavior from the experimental data, the last step that remains to be done is to fit a function for the strain-hardening $\tilde{\Theta}$ to insert into Eq. 6, which yields the measured total displacement after summation. An expression of the Ludwik's equation type was used for the true stress-strain curves:

$\sigma = E\epsilon$ for $\sigma < \sigma_y$ $\sigma = \sigma_y + A\epsilon_p^n$
for $\sigma > \sigma_y$, with $\epsilon_p = \epsilon - \epsilon_e$ (7)

which yields:

$$\tilde{\Theta} = \frac{d\sigma}{d\epsilon} = \frac{d\sigma}{d\epsilon_e} = E \qquad \text{for } \sigma < \sigma_y$$

$$\tilde{\theta} = \frac{d\sigma}{d\epsilon} = \frac{E}{1+\frac{E}{nA^{\frac{1}{n}}}(\sigma-\sigma_y)^{(\frac{1-n}{n})}} \qquad \text{for } \sigma > \sigma_y \qquad (8)$$

The previous equation shows that one can express $\tilde{\theta}$ in function of the stress, which in turn is a function of the load. Thus for each layer and load increment, one has to replace $\tilde{\theta}_{ji}$ in Eq, 6 by Eq. 8. In principle, the Young's modulus, the yield stress σ_y and the strain-hardening coefficients *A* and *n* have to be fitted in order to adjust the calculated displacement to the experimental one using Eq. 6. It has to be emphasized here that the elastic modulus obtained by this procedure does not yield the actual Young's modulus *E*. Indeed, the detailed finite element analysis of Yang *et al* [11], performed for elastic deformation demonstrated that one measures a relaxed modulus E_0 instead of *E*, with a ratio E/E_0 strongly dependent on the geometry of the micro-pillar and that can be as large as 1.8. We found a similar result, namely the elastic part of the micro-compression tests could be best fitted in a first step with a relax modulus E_0 that was such that E/E_0 = 1.7-1.8. For the plastic part of the deformation, it is easy to get a good estimate of the yield stress σ_y. It simply consists in determining the yield load and dividing it by the upper cross-section of the micro-pillar, which is the smallest and which yields at the first place (see Figure 4 and Table 1). The plastic zone propagates through the specimens upon additional loading. In the third step, the strain-hardening coefficient *A* and *n*, as well as σ_y, are adjusted to fit the displacement by using the least squared residuals method.

In Figure 6 below, we show two typical examples of analysis of micro-pillars: one for unirradiated and one for irradiated Eurofer97. The displacements were calculated by fitting E_0, σ_y, *A* and *n* described above. The fitting parameters are indicated in Table 2.

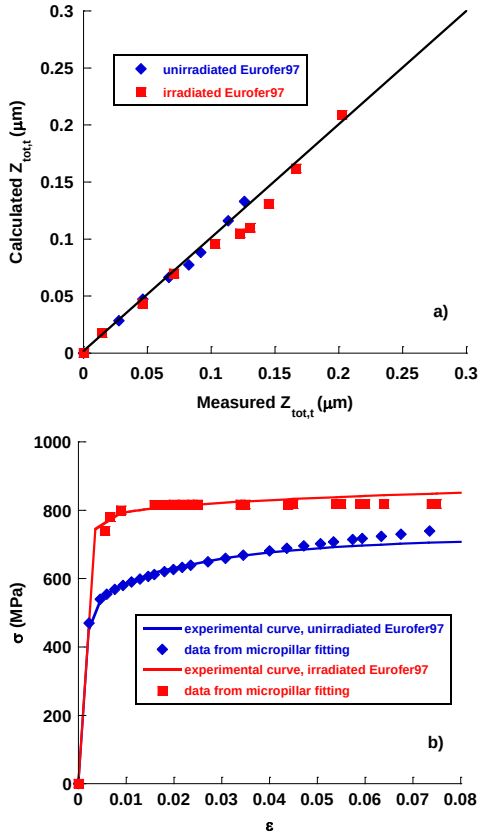

Figure 6: a) Reconstruction of the total displacements imposed on the top of the micro-pillar by fitting the constitutive parameters for unirradiated and irradiated Eurofer97. b) Comparison between the fitted constitutive behaviors and the actual ones.

Table 2: Fitting parameters to reconstruct the displacement curve of Figure 6.

	σ_y (MPa)	A (MPa)	n	E/E_0
Unirradiated Eurofer97	470	740	0.38	1.7
Irradiated Eurofer97	745	236	0.36	1.8

As can be seen, the one-to-one correspondence between the measured displacement and the calculated ones obtained for the sets of E_0, σ_y, A and n parameters reproduce well the true stress-

strain curves $\sigma(\varepsilon)$ up to strains of about 5%. For the unirradiated Eurofer97, there is a direct comparison between the adjusted and the experimental tensile $\sigma(\varepsilon)$ curves. Again such a direct comparison could not be done for the irradiated Eurofer97 since the tensile curve exhibit less than 2% of uniform elongation. However, the true stress-strain curves $\sigma(\varepsilon)$ deduced from the micro-pillar analysis compared very well with those used to reconstruct the necking behavior of the tensile curves present in**Error! Bookmark not defined.**. While the proposed analysis of the micro-pillar is simple and powerful, it is limited to about 5% of strain. Such a limitation is related to the fact that after a certain amount of compression, the deformation does not occur any more as described. As soon as the plastic zone has propagated through the entire micro-pillar, the previous analysis cannot be regarded as a reasonable approximation: the substrate begins to deform plastically and the stress state in the micro-pillar is not dominated by the normal component any more. However, at larger deformation, the true stress-strain curves $\sigma(\varepsilon)$ can be fitted with finite element simulation for strain much larger than 5%, using an inverse numerical method to reconstruct the load-displacement curve of the micro-pillar. However, it is worth outlining that the analytical method proposed in this paper allows determining the yield stress and the initial part of the strain-hardening very precisely.

References

1. CP Frick, BG Clark, S Orso, AS Schneider, E Arzt. Mater. Sci. Eng. A. 2008; 489: 319.
2. JR Greer, WD Nix. Phys. Rev. B. 2006; 73: 245410.
3. MD Uchic, DM Dimiduk, JN Florando, WD Nix. Science. 2004; 305: 986.
4. DM Dimiduk, MD Uchic, TA Parthasarathy. Acta Materialia. 2005; 53: 4065.
5. H Fei, A Abraham, N Chawla, H Jiang. Journal of Applied Mechanics. 2012; 79: 061011-1.
6. P Hosemann, E Stergar, L Peng, Y Dai, SA Maloy, et al. Journal of Nuclear Materials. 2011; 417: 274.
7. B van der Schaaf, F Tavasolli, C Fazio, E Rigal, E Diegele, et al. Fusion Engineering and Design. 2003; 69: 197.

8. N Ilchuk, P Spätig, GR Odette. Journal of Nuclear Materials. 2013; 442: S58.
9. C Shin, S Lim, H Jin, P Hosemann, J Kwon. Journal of Nuclear Materials. 2014; 444: 43.
10. IN Sneddon. International Journal of Engineering and Science. 1965; 3: 47.
11. Y Yang, JC Ye, J Lu, FX Liu, PK Liaw. Acta Materiala. 2009; 57: 1613.